

Detecting Outliers with Foreign Patch Interpolation

Jeremy Tan

Benjamin Hou

James Batten

Huaqi Qiu

Bernhard Kainz

j.tan17@imperial.ac.uk

Imperial College London, SW7 2AZ, London, UK

Abstract

In medical imaging, outliers can contain hypo/hyper-intensities, minor deformations, or completely altered anatomy. To detect these irregularities it is helpful to learn the features present in both normal and abnormal images. However this is difficult because of the wide range of possible abnormalities and also the number of ways that normal anatomy can vary naturally. As such, we leverage the natural variations in normal anatomy to create a range of synthetic abnormalities. Specifically, the same patch region is extracted from two independent samples and replaced with an interpolation between both patches. The interpolation factor, patch size, and patch location are randomly sampled from uniform distributions. A wide residual encoder decoder is trained to give a pixel-wise prediction of the patch and its interpolation factor. This encourages the network to learn what features to expect normally and to identify where foreign patterns have been introduced. The estimate of the interpolation factor lends itself nicely to the derivation of an outlier score. Meanwhile the pixel-wise output allows for pixel- and subject- level predictions using the same model.

Keywords: Outlier Detection, Medical Imaging, Self-supervised Learning

1. Introduction

Outliers in medical data can range from obvious lesions to subtle artifacts. This wide range can make it difficult for a single detection system to identify all irregularities. Moreover, examples of outliers are often not available before testing takes place. This makes it difficult to use conventional classification methods that rely on training data to learn how to recognize test images that come from the same distribution. Without knowing what to look for, this task can be challenging even for human radiologists. For example, when focused on a lung nodule detection task, 83% of radiologists failed to notice a gorilla superimposed on the image (Drew et al. (2013)). This indicates that human attention can cause even experts to be blind to unexpected stimuli. It is infeasible to have radiologists repeatedly scan for every conceivable irregularity. As such, there may be an opportunity for automated systems to support detection, especially if these tools can offer a complementary view of the data.

Recent works have used neural networks to create high performance image recognition systems. These systems typically learn to recognize different image classes based on features that distinguish them from each other. However, outlier classes are not available in during training, so it is not known *a priori* which features will be most relevant.

To circumvent this issue, reconstruction-based methods (Baur et al. (2020); Zimmerer et al. (2019); Alex et al. (2017); Schlegl et al. (2017)) aim to learn a complete model of the normal data. Abnormalities are then found by comparing the original image to its reconstruction. A key limitation of this approach is that it directly compares pixel intensities under the assumption that intensity differences will be proportional to abnormality.

We propose a self-supervised task to train a model to learn where and to what degree a foreign pattern has been introduced. The goal is to encourage the model to learn what features to expect normally, given the context, and to be sensitive to subtle irregularities.

We evaluate this approach on an internal evaluation set with synthetic abnormalities and submitted the technique to the 2020 MICCAI MOOD challenge (Zimmerer et al. (2020)) where it ranked first in both sample and pixel level tasks.

2. Related Work

Out-of-distribution (OOD) detection is a broad topic discussed by many communities (Pimentel et al. (2014); Pang et al. (2020)). Depending on the context, an OOD sample may contain minute defects or completely unrelated content. It is not always easy to formally define what constitutes an OOD sample, especially without any reference examples. This makes the task inherently heuristic and each approach must accept some assumptions which will impact its ability to detect different types of outliers. As such, one of the goals is to choose assumptions that will generalize as broadly as possible and be sensitive to the types of outliers that are of most interest. Most existing methods detect outliers based on reconstruction error, embedding space distances, or more recently, performance on self-supervised tasks. For the purpose of fair comparison, we will restrict discussion to methods that use only normal data without any examples from other classes.

Reconstruction-based methods attempt to reproduce the image using a model of the normal data. This model may be characterised by the bottleneck of an autoencoder (Baur et al. (2020)) or variational autoencoder (VAE) (Zimmerer et al. (2019)) or by the latent space of a generative adversarial network (GAN) (Alex et al. (2017); Schlegl et al. (2017)). The reconstruction error is then used to measure abnormality. These methods treat all intensity differences between a test image and it’s reconstruction equally. However, in e.g. a brain-imaging model, a hypo-intensity in the white matter may have a very different meaning from a hyper-intensity appearing in the ventricles. Likewise, small differences distributed randomly across the image may not mean the same thing as differences in correlated locations, e.g. along a tissue boundary.

To overcome these limitations, embedding-based methods try to look at distances in a semantic latent space. These methods learn to map the training samples to a compact sphere (Ruff et al. (2018)). However, without any examples of outliers in the training data, this latent space may accentuate the wrong features, i.e. variations within the normal data that are class invariant. Some embedding approaches introduce a disjoint set of outlier

examples (Bozorgtabar et al. (2020)) to overcome this issue. However in this work we focus on methods using only normal data.

Self-supervised methods have recently become a popular approach for unsupervised feature learning, especially variants of contrastive predictive coding (CPC) (Oord et al. (2018); Hénaff et al. (2019)). Self-supervised methods have also been used for outlier detection (Golan and El-Yaniv (2018)), in some cases also combined with CPC (Tack et al. (2020)). The main principle underlying many of these methods is to transform the images (e.g. rotation) and train a network to identify the transformation. This will sensitize the network to any features that change consistently with the transformation. For example, the brainstem (in a coronal view) may provide a reliable signal for predicting image rotation. However, if the brainstem structure is missing or occluded, the prediction accuracy may go down, indicating a potential outlier. This approach works well for recognizing key characteristics present in normal data. However, in medical images many pathological outliers may still conform to the same global structure as normal data.

We propose a self-supervised task that is more sensitive to subtle irregularities because 1) these may be more medically relevant and 2) detecting more fine-grained outliers may be more useful to radiologists since these typically require more intense scrutiny, time and energy to detect.

3. Method

Most self-supervised methods train a network on a proxy task (e.g. identifying geometric transformations (Golan and El-Yaniv (2018))) and subsequently measure abnormality as *failure* to perform this task. Many of these tasks are helpful for detecting the presence (or absence) of prominent structures that appear in the normal class. But medical images often contain more fine-grained outliers, where most major structures are still intact. As such, we propose a patch-level self-supervision task.

To create a variety of subtle outliers we extract the same patch from two independent subjects and replace the patch with an interpolation between both patches. The operation is shown in Eqn. 1 where A and B are independent samples, i refers to individual pixels in a patch h , and α is the interpolation factor. The patch size, h_s , patch center coordinates, h_c , and the interpolation factor are all randomly sampled from uniform distributions (Eqn. 2-4). Patches are square unless truncated by image boundaries or in pixels where A and B have the same value. Patch width ranges between 10% and 40% of the image width, d .

$$A'_i = (1 - \alpha)A_i + \alpha B_i, \forall i \in h \quad (1)$$

$$h_s \sim U(0.1 \cdot d, 0.4 \cdot d) \quad (2)$$

$$h_c \sim U_2(0.1 \cdot d, 0.9 \cdot d) \quad (3)$$

$$\begin{aligned} \alpha &\sim U(0, 1) \text{ for continuous or} \\ \alpha &\in \{0, 0.25, 0.50, 0.75, 1\} \text{ for discrete} \end{aligned} \quad (4)$$

Although A and B are both normal on their own, the differences between them will cause the interpolation, A' , to have artificial defects. We train a network to estimate where, and to what degree, a foreign pattern has been introduced. Given A' as input, the corresponding label includes the patch, h , and the interpolation factor, α , in the form of pixel-level values (Eqn. 5). The loss is thus a pixel-wise regression if α is continuous, or a pixel-wise classification if α is discrete. In both cases a standard cross entropy loss is used (Eqn. 6-7, where f represents the model). During testing, an abnormality score is derived directly from the model’s estimate of the interpolation factor α . Examples of A , A' , and corresponding labels are shown in Figure 1.

$$\alpha_i = \begin{cases} \alpha, & \text{if } i \in h \text{ and } A_i \neq B_i \\ 0, & \text{otherwise} \end{cases} \quad (5)$$

$$\mathcal{L}_{\text{bce}}(A', \alpha_i, f) = -\alpha_i \log(f(A')) - (1 - \alpha_i) \log(1 - f(A')) \quad (6)$$

$$\mathcal{L}_{\text{cce}}(A', \alpha_i, f) = -\sum_{c=1}^{N=5} \alpha_{i,c} \log(f(A')) \quad (7)$$

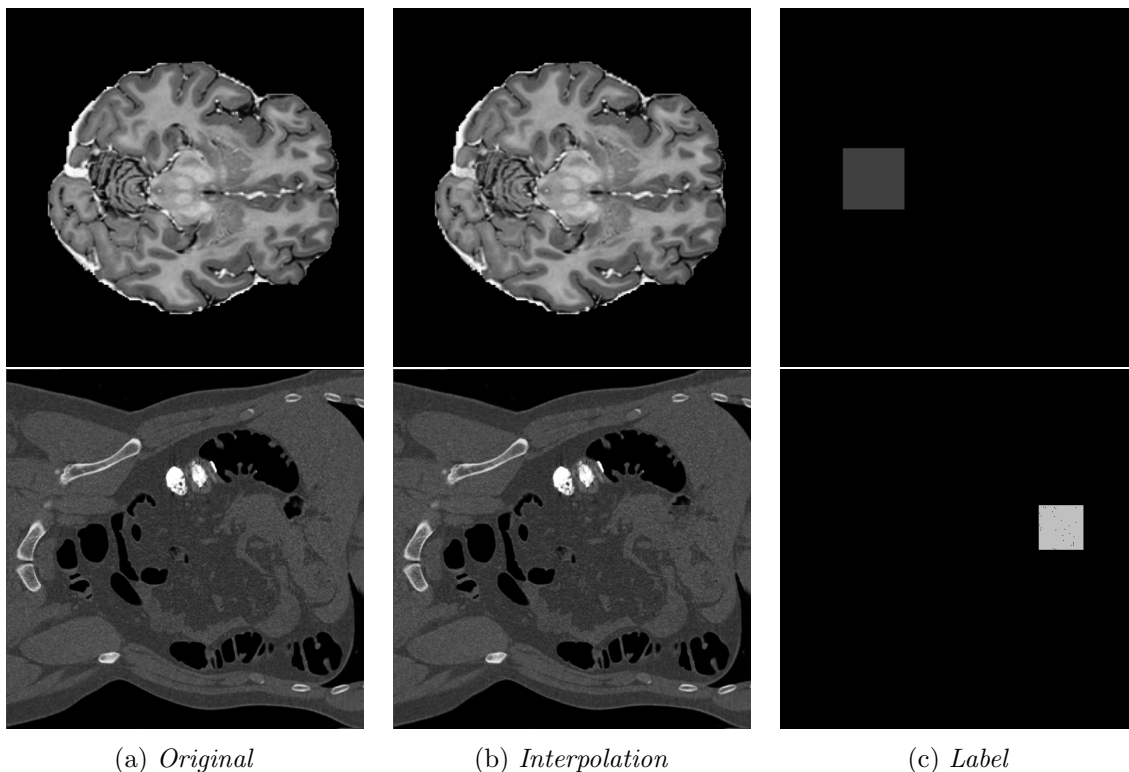


Figure 1: *Examples of foreign patch interpolation in brain and abdominal data. More examples are given in Appendix A and B.*

ARCHITECTURE:

The network architecture is a wide residual encoder-decoder. The encoder portion is a standard wide residual network (Zagoruyko and Komodakis (2016)) with a width of 4 and a depth of 14 for brain data (256x256) and 16 for abdominal data (512x512). The decoder follows the same structure as the encoder but in reverse. The terminating activation is sigmoid in the case of continuous α or softmax with the appropriate number of output channels for discrete α .

TRAINING:

Each model is trained for 50 epochs using Adam (Kingma and Ba (2014)) with a learning rate of 10^{-3} . After regular training, an additional training phase is performed for stochastic weight averaging (Izmailov et al. (2018)). Stochastic gradient descent (Robbins and Monro (1951)) is used with a cyclic learning rate oscillating in the range $[10^{-4}, 10^{-3}]$. The varying learning rate helps the model to escape minima and settle in new ones. The parameters are saved whenever the learning rate reaches a minimum. Then the final model is consolidated by taking the mean of all saved minima. Stochastic weight averaging has been shown to give better generalization (Izmailov et al. (2018)) and approximates ensembling methods without needing to increase model capacity.

3.1 Evaluation

The data used in this work comes from the medical out-of-distribution (MOOD) analysis challenge (Zimmerer et al. (2020)). It includes 800 brain MRI volumes (256x256x256) and 550 abdominal CT volumes (512x512x512). All samples are assumed to be healthy with no abnormalities. Since no test data is provided, we reserve 10% of the data as healthy test cases and we use 30% of the data to create anomalous test cases. The remaining 60% of the data is used for training. To create the anomalous test set, we synthesize five types of outliers. In each case a sphere of random size and location is selected within each volume; the pixels within that sphere are altered in one of five ways listed below. An example of a sink/source synthetic outlier is given in Figure 2. Performance is evaluated using average precision (AP).

- Uniform addition - a sphere of uniform intensity is added to the image;

$$A'_i = A_i + n, \forall i \in h, \text{ where } n \sim \mathcal{N}(0, 1) \quad (8)$$

- Noise addition - a sphere of random intensities is added to the image;

$$A'_i = A_i + n_i, \forall i \in h, \text{ where } n_i \sim \mathcal{N}(0, 1) \quad (9)$$

- Sink/source deformation - pixels are shifted toward/away from the center of the sphere;

$$\begin{aligned}
 A'_I &= A_V, \forall I \in h, \text{ where } I = (i, j, k) \text{ and} \\
 V &= \begin{cases} h_c + s(I - h_c), & \text{for source} \\ I + (1 - s)(I - h_c), & \text{for sink} \end{cases} \\
 \text{and } s &= \left(\frac{\|I - h_c\|_2}{\frac{h_s}{2}} \right)^2
 \end{aligned} \tag{10}$$

- Uniform shift - pixels in the sphere are resampled from a copy of the volume which has been shifted by a random distance in a random direction;

$$\begin{aligned}
 A'_{i,j,k} &= A_{i+a, j+b, k+c} \forall i, j, k \in h, \\
 \text{where } a, b, c &\sim \sigma \mathcal{U}(0.02 \cdot d, 0.05 \cdot d) \\
 \text{and } \sigma &= \begin{cases} +1, & \text{with prob. } \frac{1}{2} \\ -1, & \text{with prob. } \frac{1}{2} \end{cases}
 \end{aligned} \tag{11}$$

- Reflection - pixels in the sphere are resampled from a copy of the volume that has been reflected along an axis of symmetry.

$$\begin{aligned}
 A'_{i,j,k} &= A_{i,d-j,k} \forall i, j, k \in h, \\
 \text{where } d &\text{ is image width}
 \end{aligned} \tag{12}$$

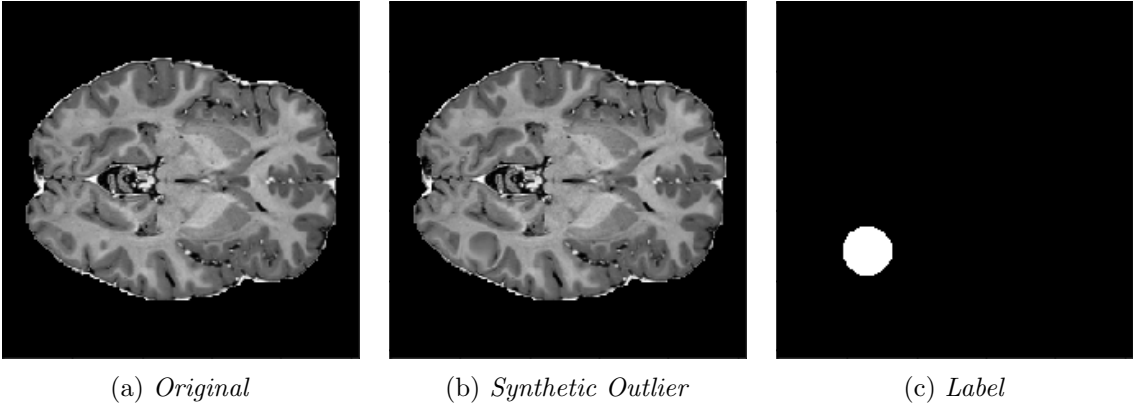


Figure 2: *Example of sink/source deformation used to synthesize an outlier. All types of synthetic outliers are displayed in Appendix C.*

4. Results

Using the synthetic test data described in Section 3.1, we evaluate the method’s ability to detect different types of outliers. Figure 3 displays the model’s response to a sink/source deformation outlier and a normal sample. The plot includes abnormality scores for individual slices across the entire volume. Slices that include the artificially deformed sphere produce a strong and consistent activation (Figure 3, red). Meanwhile, normal slices elicit only weak activations (Figure 3, blue).

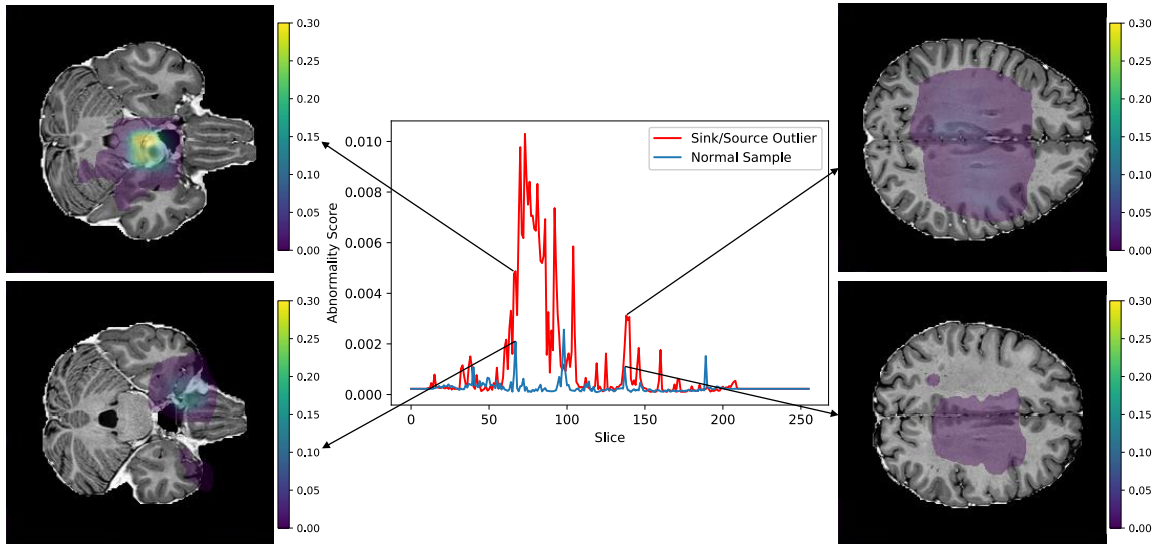


Figure 3: *Abnormality score, averaged across each slice in the volume, for a normal sample and a sink/source deformation outlier. The model gives clear and consistent activation for slices with deformation (red). Pixel-level activation maps indicate strong activation around the bulbous deformation (top left image). Normal slices contain only weak activations.*

We perform an ablation study by modifying the self-supervision task. A ‘binary’ model is trained using a binary interpolation factor ($\alpha \in \{0, 1\}$). For a ‘continuous round-up’ model, the training examples are generated using a continuous interpolation factor ($\alpha \in [0, 1]$), but the label supplied to the model is binary ($\alpha = 1$ if $\alpha > 0$). We also compare continuous and discrete configurations ($\alpha \in \{0, 0.25, 0.50, 0.75, 1\}$) as well as the application of stochastic weight averaging. Figure 4 displays the results for individual types of outliers and also overall sample and pixel level scores. Note that the overall scores (Figure 4, blue and green) are calculated using all outlier samples and all normal samples, so the class distribution is different from the individual scores. The binary and continuous round-up models are not able to detect the outliers in the test set effectively. Both continuous and discrete models achieve high performance. However, the low performance of the continuous stochastic weight averaged model may indicate that optimization is less stable for the continuous task. In contrast, stochastic weight averaging does not hurt performance for the discrete model and can substantially improve pixel-level scores.

The abdominal models were trained in a similar manner and the discrete stochastic weight averaged model achieved the best overall performance. Table 1 shows the perfor-

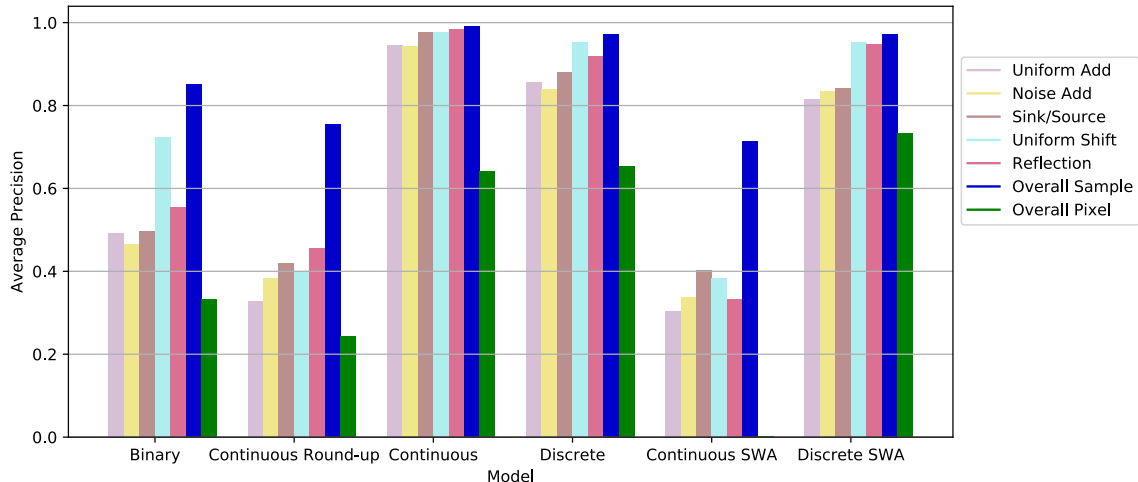


Figure 4: Average precision for brain data using different model configurations.

mance of the final selected models which are both trained using the discrete stochastic weight averaged configuration.

For reference, two baseline methods have been evaluated on the same data. The first baseline, deep support vector data description (SVDD) (Ruff et al. (2018)), is an embedding-based approach that learns a compact representation of the normal data. The second baseline is a reconstruction-based method using a convolutional autoencoder (CAE) (Masci et al. (2011)). The CAE baseline reconstructs images using features that are learned from normal data. Errors in the reconstruction are considered abnormal.

Table 1: Average precision for final brain and abdominal models using synthetic evaluation data. For reference, two baseline methods are evaluated on the same data.

Anatomy	Method	Sample-level AP	Pixel-level AP
Brain	Deep SVDD (Ruff et al. (2018))	0.7695	–
	CAE (Masci et al. (2011))	0.7617	0.0120
	FPI (ours)	0.9723	0.7319
Abdomen	Deep SVDD (Ruff et al. (2018))	0.8318	–
	CAE (Masci et al. (2011))	0.7378	0.0096
	FPI (ours)	0.8854	0.6229

In addition to the synthetic test set, which only includes local abnormalities, we provide examples of global abnormalities in Figure 5. A normal example produces virtually no activation in its canonical orientation (Figure 5, left most image in (a)). However, rotating the sample produces scattered activations (Figure 5, (a)), throughout the entire volume (Figure 5, (c)). Blurring or substituting different anatomy produces even stronger activations (Figure 5, (b)).

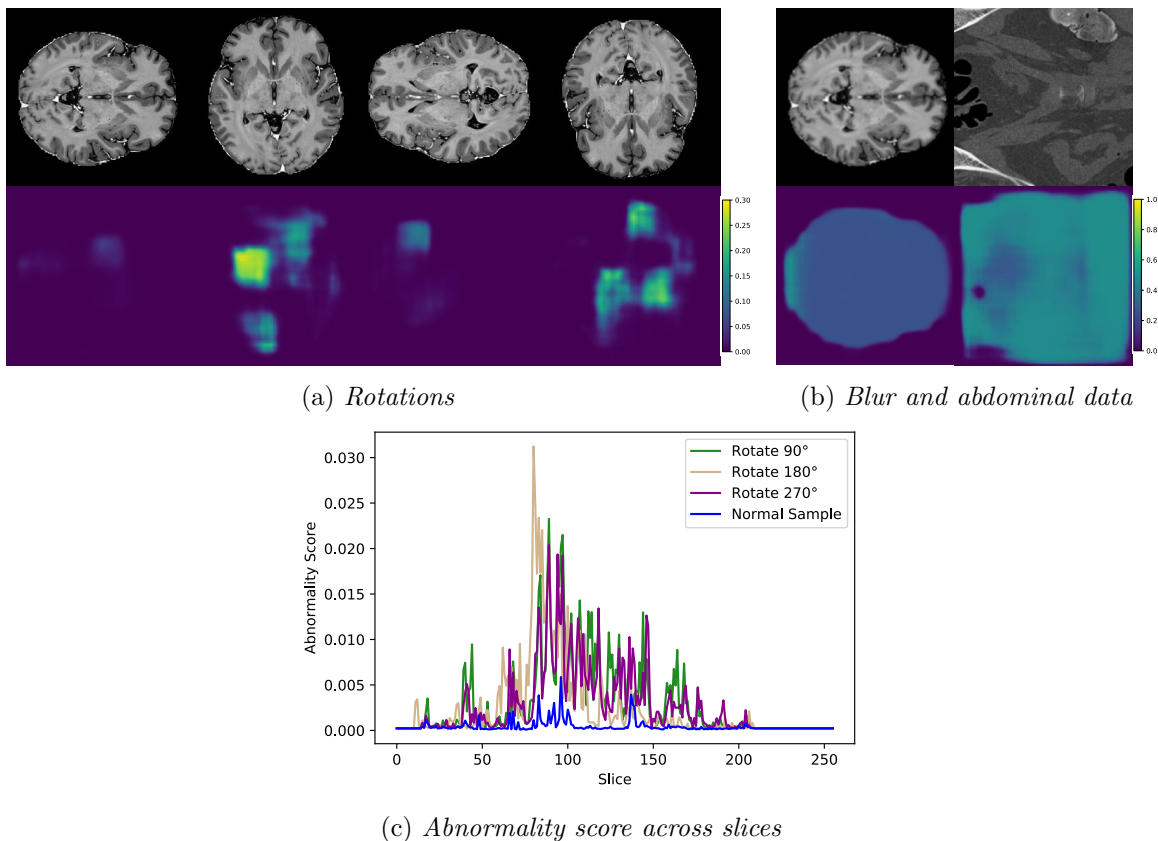


Figure 5: *Examples of global outliers. (a) Original normal sample (top left) and rotations. (b) Gaussian blur ($\sigma = 1$) and abdominal data. Note the change of scale in activation maps. (c) Abnormality score across slices for different rotations.*

5. Discussion

The proposed method uses a simple self-supervised task to simulate subtle irregularities in the image. We evaluate the method using a disjoint set of abnormalities, synthesized in our test set. The results indicate that this single task can sensitize a model to a range of outlier types. Our ablation study suggests that two aspects of this task are important, exposure and difficulty. Using a non-binary interpolation factor exposes the network to a range of abnormalities with different levels of subtlety. In contrast, training with a binary interpolation factor gives less variety of training examples. This leads to poorer generalization to the synthetic test data (Figure 4). But exposure to subtle artifacts is not sufficient on its own. The task of estimating the *value* of the interpolation factor is also crucial. If training examples are created using a varying interpolation factor ($\alpha \in [0, 1]$), but the task is simplified by rounding the label to a binary value ($\alpha = 1$ if $\alpha > 0$) then generalization is also poor (Figure 4). The difficulty and variety of the proposed task allow it to achieve high performance in both continuous and discrete α settings. However, training with a discrete interpolation factor appears to be more stable and is thus easier to combine with stochastic weight averaging. While stochastic weight averaging does not bestow much

benefit at the sample-level, it is able to increase the pixel-level AP from 0.6539 to 0.7319 (Figure 4).

Due to the nature of the self-supervised task and the synthesized outliers, one concern is that the network may only detect discontinuities in image intensity. However, Figure 5 demonstrates that even when there are no discontinuities or alterations to pixel intensities, the model can still identify irregularities. The detection of rotated samples, shown in (a) and (c), indicates that the network is sensitive to deviations from the norm, even when there are no discontinuities. This implies that the self-supervised task helps the network to learn the normal appearance of anatomy to some extent. And as a result, the model interprets deviations from that expectation as foreign patterns being introduced ($\alpha > 0$).

A major difference between this work and reconstruction-based methods is that we focus on subtle irregularities. In a reconstruction-based approach, the abnormality score is directly proportional to the intensity differences between the test image and its reconstruction. Accordingly, these methods are often evaluated on gross abnormalities or hypo/hyper-intensities that are immediately noticeable, even for lay observers. Outliers that do not contain such obvious intensity differences may be harder to detect using a reconstruction-based approach.

Our training examples (Figure 1) and synthesized test outliers (Figure 2) contain abnormalities that can be difficult to identify, even when the label and original image are provided. Such subtle abnormalities can be harder to detect using existing baseline methods (Table 1). Our method can complement reconstruction-based approaches and excels in cases that can be difficult and time consuming for radiologists.

6. Conclusion

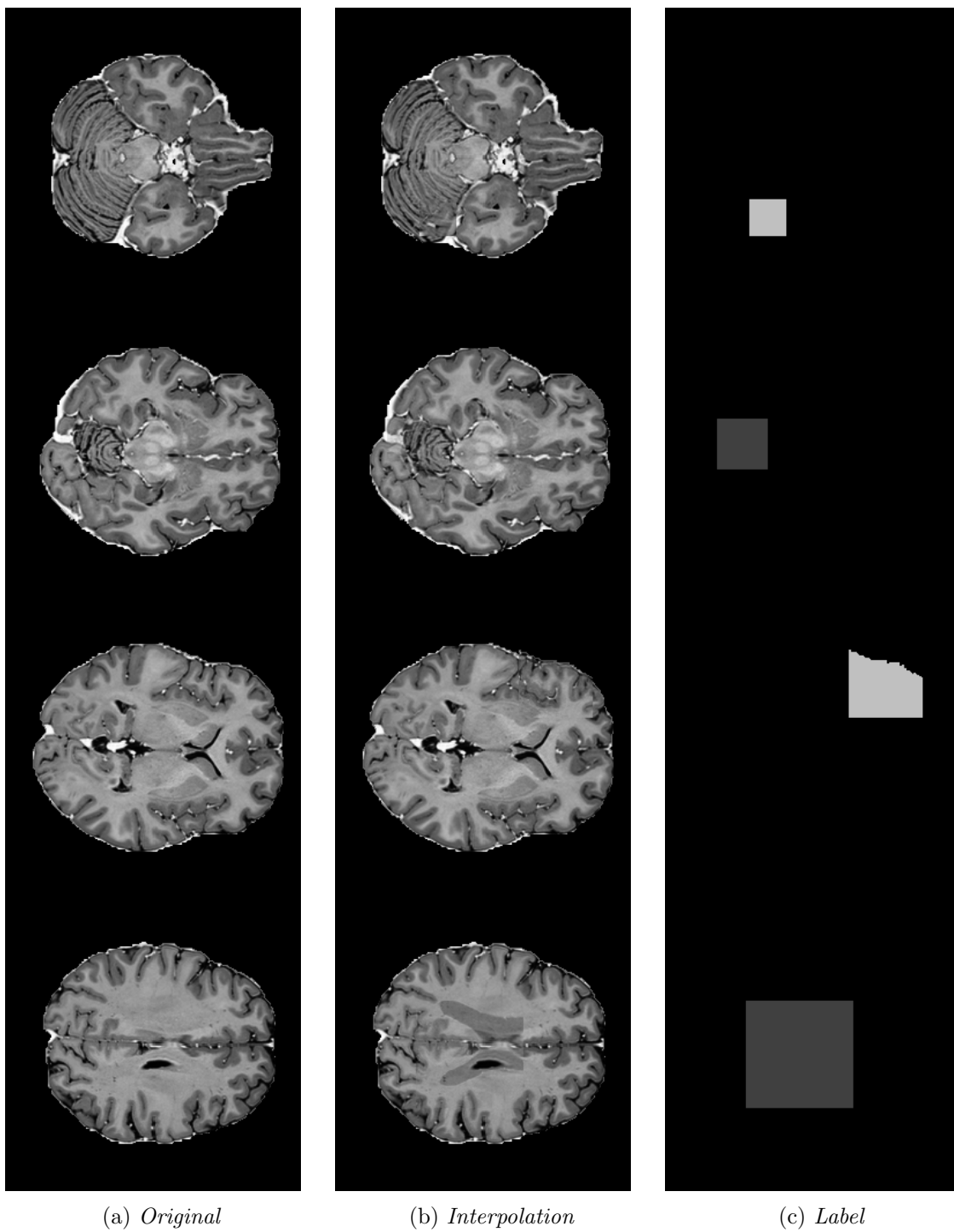
We propose a self-supervision framework for detecting fine-grained abnormalities, common in medical data. Foreign patterns are drawn from independent subjects and used to simulate abnormalities. The network is trained to detect where and to what degree a foreign pattern has been introduced. The resulting model is able to generalize to a wide range of subtle irregularities and achieved the highest rank in the 2020 MICCAI MOOD challenge (Zimmerer et al. (2020)) in both sample and pixel level tasks.

The goal of future work is to extend to cases where there is less structural consistency between samples and ultimately to reduce the burden placed on radiologists.

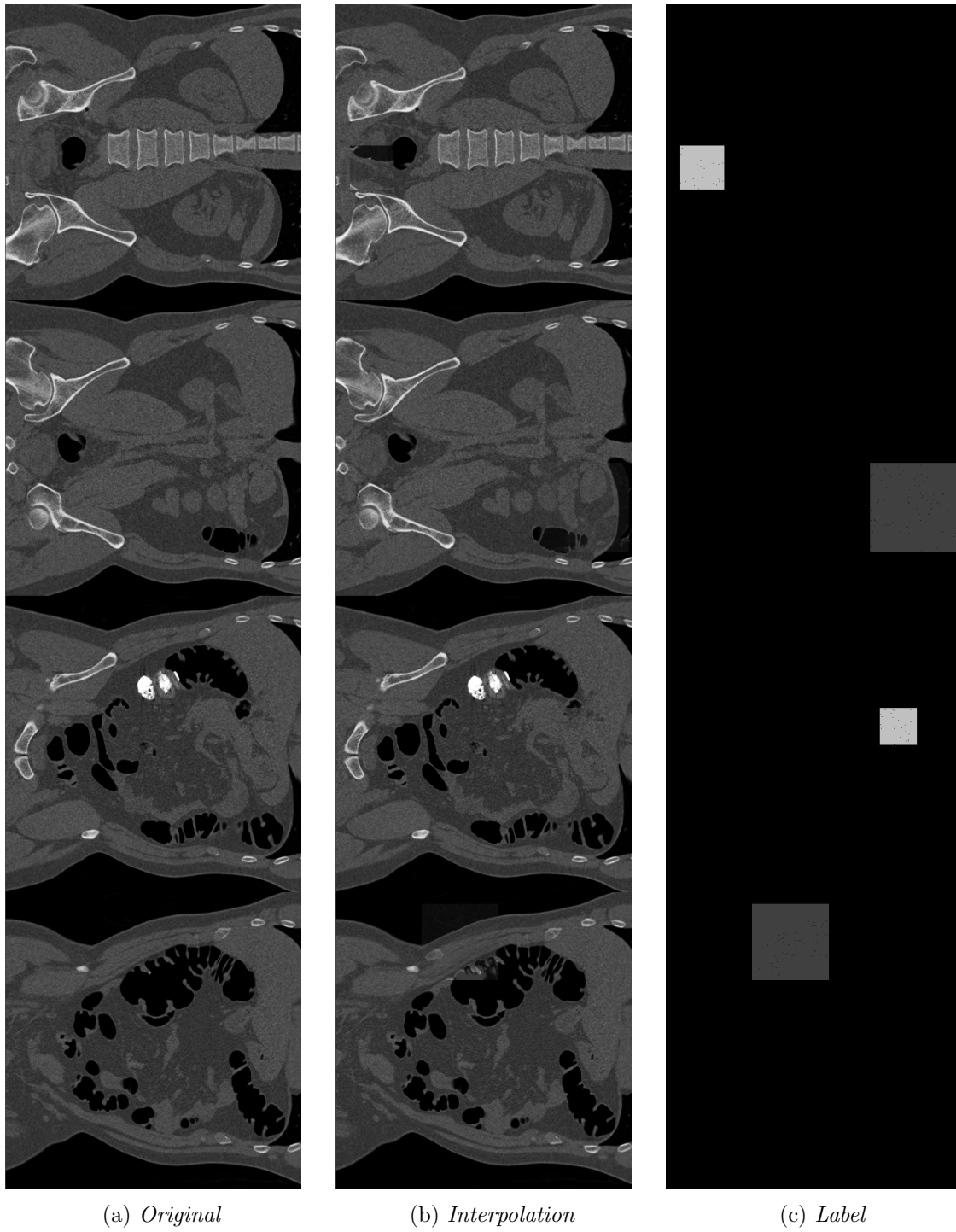
Acknowledgments

JT is supported by an Imperial College London President’s Scholarship. This work was supported by the London Medical Imaging & AI Centre for Value Based Healthcare (104691), EP/S013687/1, EP/R005982/1 and Nvidia for the ongoing donations of high-end GPUs.

Appendix A. Foreign Patch Interpolation in Brain Images

Figure 6: *Examples of brain images with foreign patches.*

Appendix B. Foreign Patch Interpolation in Abdominal Images

Figure 7: *Examples of abdominal images with foreign patches.*

Appendix C. Examples of Synthetic Outliers

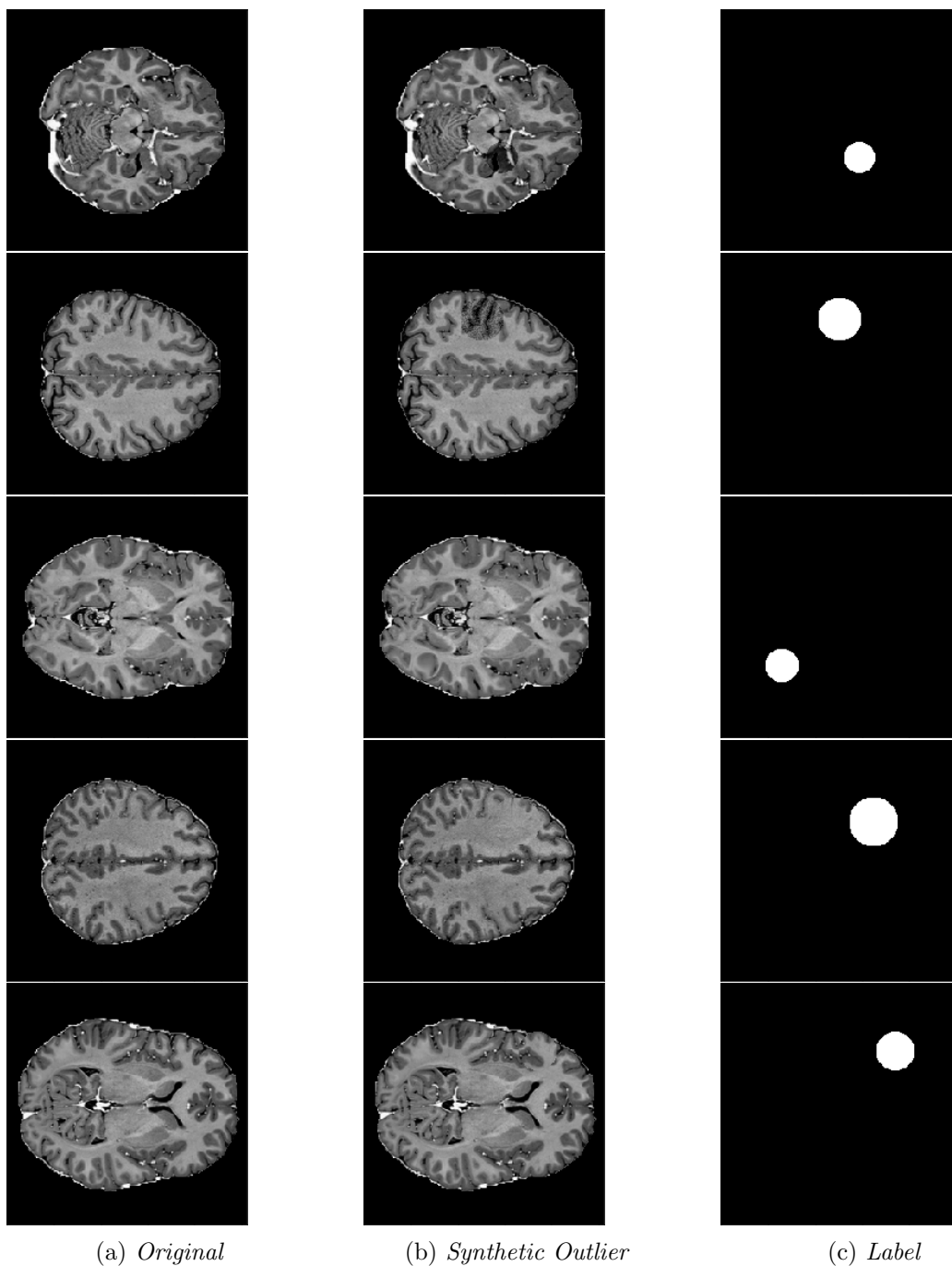


Figure 8: Each row shows one type of synthetic outlier. From top to bottom these are uniform addition, noise addition, sink/source deformation, uniform shift, and reflection.

References

- Varghese Alex, Mohammed Safwan KP, Sai Saketh Chennamsetty, and Ganapathy Krishnamurthi. Generative adversarial networks for brain lesion detection. In *Medical Imaging 2017: Image Processing*, volume 10133, page 101330G. International Society for Optics and Photonics, 2017.
- Christoph Baur, Benedikt Wiestler, Shadi Albarqouni, and Nassir Navab. Scale-space autoencoders for unsupervised anomaly segmentation in brain mri. In *International Conference on Medical Image Computing and Computer-Assisted Intervention*, pages 552–561. Springer, 2020.
- Behzad Bozorgtabar, Dwarikanath Mahapatra, Guillaume Vray, and Jean-Philippe Thiran. Salad: Self-supervised aggregation learning for anomaly detection on x-rays. In *International Conference on Medical Image Computing and Computer-Assisted Intervention*, pages 468–478. Springer, 2020.
- T Drew, ML Võ, and JM Wolfe. The invisible gorilla strikes again: sustained inattentive blindness in expert observers. *Psychological Science*, 24(9):1848–1853, 2013.
- Izhak Golan and Ran El-Yaniv. Deep anomaly detection using geometric transformations. In *Advances in Neural Information Processing Systems*, pages 9758–9769, 2018.
- Olivier J Hénaff, Aravind Srinivas, Jeffrey De Fauw, Ali Razavi, Carl Doersch, SM Eslami, and Aaron van den Oord. Data-efficient image recognition with contrastive predictive coding. *arXiv preprint arXiv:1905.09272*, 2019.
- Pavel Izmailov, Dmitrii Podoprikin, Timur Garipov, Dmitry Vetrov, and Andrew Gordon Wilson. Averaging weights leads to wider optima and better generalization. *Uncertainty in Artificial Intelligence*, 2018.
- Diederik P Kingma and Jimmy Ba. Adam: A method for stochastic optimization. *arXiv preprint arXiv:1412.6980*, 2014.
- Jonathan Masci, Ueli Meier, Dan Cireşan, and Jürgen Schmidhuber. Stacked convolutional auto-encoders for hierarchical feature extraction. In *International conference on artificial neural networks*, pages 52–59. Springer, 2011.
- Aaron van den Oord, Yazhe Li, and Oriol Vinyals. Representation learning with contrastive predictive coding. *arXiv preprint arXiv:1807.03748*, 2018.
- Guansong Pang, Chunhua Shen, Longbing Cao, and Anton van den Hengel. Deep learning for anomaly detection: A review, 2020.
- Marco AF Pimentel, David A Clifton, Lei Clifton, and Lionel Tarassenko. A review of novelty detection. *Signal Processing*, 99:215–249, 2014.
- Herbert Robbins and Sutton Monro. A stochastic approximation method. *The annals of mathematical statistics*, pages 400–407, 1951.

- Lukas Ruff, Robert Vandermeulen, Nico Goernitz, Lucas Deecke, Shoaib Ahmed Siddiqui, Alexander Binder, Emmanuel Müller, and Marius Kloft. Deep one-class classification. In *International conference on machine learning*, pages 4393–4402, 2018.
- Thomas Schlegl, Philipp Seeböck, Sebastian M Waldstein, Ursula Schmidt-Erfurth, and Georg Langs. Unsupervised anomaly detection with generative adversarial networks to guide marker discovery. In *International conference on information processing in medical imaging*, pages 146–157. Springer, 2017.
- Jihoon Tack, Sangwoo Mo, Jongheon Jeong, and Jinwoo Shin. Csi: Novelty detection via contrastive learning on distributionally shifted instances. *arXiv preprint arXiv:2007.08176*, 2020.
- Sergey Zagoruyko and Nikos Komodakis. Wide residual networks. In Edwin R. Hancock Richard C. Wilson and William A. P. Smith, editors, *Proceedings of the British Machine Vision Conference (BMVC)*, pages 87.1–87.12. BMVA Press, September 2016. ISBN 1-901725-59-6. doi: 10.5244/C.30.87. URL <https://dx.doi.org/10.5244/C.30.87>.
- David Zimmerer, Fabian Isensee, Jens Petersen, Simon Kohl, and Klaus Maier-Hein. Unsupervised anomaly localization using variational auto-encoders. In *International Conference on Medical Image Computing and Computer-Assisted Intervention*, pages 289–297. Springer, 2019.
- David Zimmerer, Jens Petersen, Gregor Köhler, Paul Jäger, Peter Full, Tobias Roß, Tim Adler, Annika Reinke, Lena Maier-Hein, and Klaus Maier-Hein. Medical out-of-distribution analysis challenge, March 2020. URL <https://doi.org/10.5281/zenodo.3784230>.